Structural Stability of Turbulent Jets

Brian F. Farrell

Division of Engineering and Applied Sciences, Harvard University, Cambridge, Massachusetts

Petros J. Ioannou

Department of Physics, University of Athens, Athens, Greece

ABSTRACT

Turbulence in fluids is commonly observed to coexist with relatively large spatial and temporal scale coherent jets. These jets may be steady, vacillate with a definite period, or be irregular. A comprehensive theory for this phenomenon is presented based on the mutual interaction between the coherent jet and the turbulent eddies. When a sufficient number of statistically independent realizations of the eddy field participate in organizing the jet a simplified asymptotic dynamics emerges with progression, as an order parameter such as the eddy forcing is increased, from a stable fixed point associated with a steady symmetric zonal jet through a pitchfork bifurcation to a stable asymmetric jet followed by a Hopf bifurcation to a stable limit cycle associated with a regularly vacillating jet and finally a transition to chaos. This underlying asymptotic dynamics emerges when a sufficient number of ensemble members is retained in the stochastic forcing of the jet but a qualitative different mean jet dynamics is found when a small number of ensemble members is retained as is appropriate for many physical systems. Example applications of this theory are presented including a model of midlatitude jet vacillation, emergence and maintenance of multiple jets in turbulent flow, a model of rapid reorganization of storm tracks as a threshold in radiative forcing is passed, and a model of the quasi-biennial oscillation. Because the statistically coupled wave–mean flow system discussed is generally globally stable this system also forms the basis for a comprehensive theory for equilibration of unstable jets in turbulent shear flow.

1. Introduction

Emergence of coherent jets from relatively incoherent background velocity fields occurs in both rotating and nonrotating fluids. Examples of steady jets include the banded winds of the gaseous planets (Ingersol 1990); examples of orderly variation include the quasi-biennial oscillation (QBO) of the equatorial stratosphere (Reed and Rogers 1962), and the torsional oscillations of the solar convection zone (Vorontsov et al. 2002). Earth's midlatitude jets show a more stochastic variation of structure that nevertheless appears to be modified by feedback between the eddy field and the jets (Robinson 1991, 1996, 2000; Hartmann and Lo 1998; Feldstein 2000; Lorenz and Hartmann 2001; Watterson 2002).

The organization of jets by turbulence has been extensively studied in connection with specific occurrences of this phenomenon (Lindzen and Holton 1968; Holton and Mass 1976; Plumb and McEwan 1978; Williams 1979a,b; Hou and Farrell 1987; Lee and Feldstein 1996; Yoden 1987a,b; Panetta 1993; Ioannou and Lindzen 1994; Scott and Haynes 2000). In this work, rather than addressing a particular instance, we advance a comprehensive theory for the structure of turbulent jets. This theory of the formation and stability of jets in turbulence builds on results from stochastic turbulence modeling (Farrell and Ioannou 1993a,b, 1996; DelSole and Farrell 1996) that provide an analytic method for computing the distribution of momentum flux arising from the turbulent wave field associated with a given jet structure. In the formulation of this theory for the stability and structure of turbulent jets the momentum flux distribution from stochastic turbulence theory is coupled with the mean zonal momentum equation to produce a closed set of wave–mean flow equations. In the limit that a large number of independent eddies interact with the zonal flow the zonally averaged momentum flux is accurately approximated by the time-independent ensemble mean obtained using stochastic turbulence theory. In this limit the coupled equations become autonomous and one can determine their equilibria, which are the jets maintained by balance between the mean flow forcing and the momentum flux divergence arising from the perturbation field. The stability of these jets is a central object of our study.

The coupled equations do not support unbounded solutions even if the velocity profiles become transiently unstable in the traditional sense, that is, in the sense

Corresponding author address: Petros Ioannou, Division of Engineering and Applied Sciences, Harvard University, Pierce Hall 107D, Oxford Street Mail Area H0162, Cambridge, MA 02138.
E-mail: pji@deas.harvard.edu

that if the mean profile were frozen perturbations would grow exponentially, and the present theory provides an alternative to the Landau equation paradigm for stabilization of unstable systems. The coupled equations we study naturally exhibit the primary physical mechanism by which instabilities equilibrate in a turbulent environment, which is modification of the mean flow by the perturbation field (cf. Lindzen and Farrell 1977; Stone 1978; Schoeberl and Lindzen 1984; Gutowski 1985). This work also generalizes the theory of zonal jet vacillation, previously studied assuming deterministic interference, to include stochastic wave–mean flow processes (Pedlosky 1972, 1977; Pedlosky and Frenzen 1980; Lindzen et al. 1982).

The equilibria of the stochastic ensemble wave–mean flow system are of a new type; they are statistical equilibria of the ensemble mean perturbations and the zonal mean rather than deterministic fixed points. These equilibria are distinct from equilibria in previous studies of wave–mean flow interaction involving fixed point solutions of deterministic systems (cf. Charney and DeVore 1979).

Two concepts of stability are relevant to the jet equilibria. The first is the stability of the structure of the equilibrium jet to imposed variations of its profile. A small variation in the shape of the jet leads to a variation in the associated eddy fields that may either bring the jet back to its original configuration or further disrupt it. In the first case the jet is stable, in the second unstable. The stability of the jet structure in this sense has been the frequent subject of observational studies. Some observational studies suggest that eddy feedback stabilizes zonal jets (Karoly 1990; Hartmann 1995; Kidson and Sinclair 1995; Hartmann and Lo 1998) while other suggest that feedbacks destabilize the zonal jets (Feldstein and Lee 1998). Lorenz and Hartmann (2001) analyze eddy feedback in an observational study of the Southern Hemisphere jet and conclude that both stabilizing and destabilizing tendencies are included in the feedback, but that stabilizing effects dominate.

The second stability concept relevant to wave–mean flow equilibria is the global structural stability of the equilibria: how the equilibria vary in type and are eventually destroyed as a function of a parameter of the system. This is the structural stability of systems as studied in dynamical system theory (Guckenheimer and Holmes 1983; Crawford 1991). We will show that there exists a parameter range in which globally attracting equilibria of the wave–mean flow system exist, and that as a parameter changes these become unstable through a bifurcation leading to periodic vacillation of the system and eventually, as the parameter further increases, to chaos.

2. Formulation of the stochastic wave–mean flow system

Consider a streamfunction perturbation field $\psi(x, y, t) = \hat{\psi}(y, t)e^{ikx}$ obeying the forced linearized barotropic perturbation equations:

$$\frac{d\hat{\psi}}{dt} = \mathbf{A}(U)\hat{\psi} + \mathbf{F}\xi(t). \tag{1}$$

The streamfunction perturbations are imposed on a zonal mean flow $U(y, t)$ and the linear operator $\mathbf{A}(U)$ governs the perturbation dynamics about this zonal mean flow; x is the zonal direction, k is the zonal wavenumber, and y is the meridional direction. The temporal structure of the forcing is assumed for simplicity to be a delta-correlated white noise process with zero mean and unit variance:

$$\langle \xi(t) \rangle = 0, \qquad \langle \xi(t)\xi^{\dagger}(s) \rangle = \mathbf{I}\delta(t - s), \tag{2}$$

where $\mathbf{I}$ is the identity matrix and the angle brackets denote an ensemble average, that is, an average over different realizations of the forcing. The spatial structure of the time-dependent forcing $\mathbf{F}\xi(t)$ is given by the structure matrix $\mathbf{F}$ so that the ensemble average of the spatial covariance matrix of the stochastic forcing is $\mathbf{Q} = \mathbf{F}\mathbf{F}^{\dagger}$ († denotes Hermitian transposition).

Perturbation dynamics in turbulent shear flow is dominated by transient growth and the excitation and damping of this linear transient growth by processes including nonlinear wave–wave interactions can be represented by a combination of stochastic driving and eddy damping (Farrell and Ioannou 1993a,b, 1994, 1995, 1998; DelSole 1996, 1999, 2001b; DelSole and Farrell 1995, 1996). The turbulence theory that results produces an accurate description of the structure and spectra of midlatitude eddies as well as their more subtle velocity covariances and this allows momentum fluxes to be accurately determined (Farrell and Ioannou 1994, 1995; Whitaker and Sardeshmukh 1998; Zhang and Held 1999; DelSole 2001a). We will assume that the perturbation field and the associated momentum transports are adequately described by this turbulence model.

The zonal mean flow evolves according to

$$\frac{dU}{dt} = \overline{vq} - r_e(U - U_e), \tag{3}$$

with zonal and meridional perturbation velocity components $u = \hat{u}e^{ikx}$ and $v = \hat{v}e^{ikx}$,

$$\hat{u} = -\frac{\partial \hat{\psi}}{\partial y}, \qquad \hat{v} = ik\hat{\psi}, \tag{4}$$

and perturbation vorticity $q = \hat{q}e^{ikx}$ defined as

$$\hat{q} = \frac{d^2\hat{\psi}}{dy^2} - k^2\hat{\psi}. \tag{5}$$

The zonal average vorticity flux appearing in (3) is given by

$$\overline{vq} = \frac{k}{2\pi}\int_0^{2\pi/k} dx\, \mathrm{Re}(\hat{v}e^{ikx})\, \mathrm{Re}(\hat{q}e^{ikx})$$

$$= -\frac{k}{2}\, \mathrm{diag}[\mathrm{Im}(\hat{\psi}\hat{\psi}^{\dagger})\Delta^{\dagger}], \tag{6}$$

where in the last expression $\hat{\psi}$ is treated as a column vector, diag denotes the diagonal of a matrix and $\Delta^\dagger$ is the adjoint of the Laplacian (in which the appropriate problem-specific boundary conditions are incorporated). The zonally averaged mean flow relaxes to a background radiative equilibrium flow U_e at rate r_e.

Using (1), (3), and (6) the system of equations governing the coupled evolution of the zonal mean flow and the perturbation field under the action of a single realization of the forcing is

$$\frac{d\hat{\psi}}{dt} = \mathbf{A}(U)\hat{\psi} + \mathbf{F}\xi(t), \tag{7a}$$

$$\frac{dU}{dt} = -\frac{k}{2} \, \text{diag}(\text{Im}(\hat{\psi}\hat{\psi}^\dagger)\Delta^\dagger] - r_e(U - U_e). \tag{7b}$$

Assume now that we have N statistically independent realizations of the forcing around a latitude circle so that the spatial autocorrelation scale of the perturbation field is L/N, where L is the length of a latitude circle. In such a case the evolution of the coupled system consisting of the N independent realizations of the perturbation fields, $\hat{\psi}^i$, and the zonal flow is governed by the equation set:

$$\frac{d\hat{\psi}^i}{dt} = \mathbf{A}(U)\hat{\psi}^i + \mathbf{F}\xi^i(t), \qquad (i = 1, \ldots, N) \tag{8a}$$

$$\mathbf{C} = \frac{1}{N} \sum_{i=1}^{N} \hat{\psi}^i\hat{\psi}^{i\dagger}, \tag{8b}$$

$$\frac{dU}{dt} = -\frac{k}{2} \, \text{diag}[\text{Im}(\mathbf{C})\Delta^\dagger] - r_e(U - U_e), \tag{8c}$$

where ξ^i is the ith forcing realization and $\mathbf{C}$ is the zonal and N-ensemble averaged covariance matrix. The coupled system (8) can be written more suggestively in the form

$$\frac{d\mathbf{C}}{dt} = \mathbf{A}\mathbf{C} + \mathbf{C}\mathbf{A}^\dagger + \mathbf{Q}^N(t) \tag{9a}$$

$$\frac{dU}{dt} = -\frac{k}{2} \, \text{diag}[\text{Im}(\mathbf{C})\Delta^\dagger] - r_e(U - U_e), \tag{9b}$$

in which the covariance matrix evolves according to a time-dependent Lyapunov equation (9a), that is forced by

$$\mathbf{Q}^N(t) = \frac{\sum_{i}^{N} \mathbf{F}\xi^i(t)\hat{\psi}^{i\dagger} + \hat{\psi}^i\xi^{i\dagger}(t)\mathbf{F}^\dagger}{N}. \tag{10}$$

The set of equations (9a), (9b) is not closed because the forcing $\mathbf{Q}^N(t)$ depends on the state $\hat{\psi}^i$, which must be solved explicitly, but as the number of independent realizations increases we obtain an autonomous closed set of equations. This is because as N increases the forcing $\mathbf{Q}^N(t)$ approaches the time-independent ensemble average forcing $\mathbf{Q} = \mathbf{F}\mathbf{F}^\dagger$:

$$\lim_{N\to\infty} \mathbf{Q}^N(t) \equiv \langle \mathbf{F}\xi(t)\hat{\psi}^\dagger + \hat{\psi}\xi^\dagger(t)\mathbf{F}^\dagger \rangle = \mathbf{F}\mathbf{F}^\dagger. \tag{11}$$

If we decompose $\mathbf{Q}^N(t)$ into its asymptotic form and the deviation from it

$$\mathbf{Q}^N(t) = \mathbf{Q} + \mathbf{Q}'(t), \tag{12}$$

we can estimate from the law of large numbers that the magnitude of $\mathbf{Q}'(t)$ is $O(1/N)$. Therefore, in the limit $N \to \infty$ the time-dependent forcing $\mathbf{Q}'(t) \to 0$ and the coupled equations that govern the ensemble mean system become autonomous:

$$\frac{d\mathbf{C}}{dt} = \mathbf{A}\mathbf{C} + \mathbf{C}\mathbf{A}^\dagger + \mathbf{Q}, \tag{13a}$$

$$\frac{dU}{dt} = -\frac{k}{2} \, \text{diag}[\text{Im}(\mathbf{C})\Delta^\dagger] - r_e(U - U_e). \tag{13b}$$

These two equations define a dynamical system with variables the components of the positive definite Hermitian matrix $\mathbf{C}$ and the velocity U.

A very important property of the ensemble mean equations (13a), (13b) and of their finite ensemble counterpart (8a)–(8c) is their global stability, that is, that both the perturbations field covariances and the zonal jets remain bounded for all times. The proof is given in the appendix. This global stability property of the coupled equations implies that even if the velocity profiles become transiently exponentially unstable the fluxes induced by the perturbation fields equilibrate the instabilities maintaining perturbation fields of finite variance and bounded mean winds. These coupled equations can thus produce a time-dependent equilibration of instabilities in a turbulent environment and constitute a stochastic alternative to the deterministic Landau equation paradigm for stabilization of unstable systems.

3. Equilibria of the ensemble mean coupled system and their stability

Recall that the ensemble mean evolution is governed by the coupled equations

$$\frac{d\mathbf{C}}{dt} = \mathbf{A}\mathbf{C} + \mathbf{C}\mathbf{A}^\dagger + \mathbf{Q}, \tag{14a}$$

$$\frac{dU}{dt} = -\frac{k}{2} \, \text{diag}[\text{Im}(\mathbf{C})\Delta^\dagger] - r_e(U - U_e). \tag{14b}$$

If the timescale for the covariance to converge to its asymptotic value is much shorter than the timescale for evolution of the mean flow we may assume that the covariances are functions of the instantaneous mean flow. This $\mathbf{C}(U)$ is found by solving the equilibrium form of (14a):

$$\mathbf{A}(U)\mathbf{C} + \mathbf{C}\mathbf{A}^\dagger(U) = -\mathbf{Q}. \tag{15a}$$

Under this adiabatic approximation the mean velocity evolves according to

$$\frac{dU}{dt} = -\frac{k}{2}\,\mathrm{diag}\{\mathrm{Im}[\mathbf{C}(U)]\Delta^{\dagger}\} - r_e(U - U_e), \quad (15b)$$

which is an equation only in $U(y, t)$. A roughly equivalent adiabatic assumption is commonly used to obtain a single evolution equation for zonal velocity in studies of the QBO (Lindzen and Holton 1968; Plumb and McEwan 1978).

Equations (15a), (15b) possesses equilibria consisting of velocity U_E and associated perturbation covariance $\mathbf{C}_E$ satisfying

$$\mathbf{A}(U_E)\mathbf{C}_E + \mathbf{C}_E\mathbf{A}^{\dagger}(U_E) = -\mathbf{Q},$$

$$\overline{vq}_E \equiv -\frac{k}{2}\,\mathrm{diag}[\mathrm{Im}(\mathbf{C}_E)\Delta^{\dagger}]$$

$$= r_e(U_E - U_e). \quad (16)$$

The equilibria $(U_E, \mathbf{C}_E)$ are also equilibria of the coupled system (14a), (14b) and if stable they may be found by forward integration of the time-dependent coupled equations (14a), (14b); otherwise, a root finder must be employed.

In order to determine the stability of the equilibria consider the evolution of small perturbations δU and $\delta\mathbf{C}$ imposed on the equilibrium U_e and $\mathbf{C}_E$. Because the projection operator separating out the imaginary part of $\mathbf{C}$ in the mean flow tendency equation is not analytic we must solve explicitly for the real and imaginary part of the covariances, $\delta\mathbf{C}^R$ and $\delta\mathbf{C}^I$. Expressed using the summation convention these variational equations are

$$\frac{d\delta C^R_{ij}}{dt} = A^R_{Eik}\delta C^R_{kj} - A^I_{Eik}\delta C^I_{kj} + \delta C^R_{ik}A^R_{Ejk} - \delta C^I_{ik}A^I_{Ejk}$$

$$+ \frac{\partial A^R_{Eik}}{\partial U_l}C^R_{Ekj}\delta U_l - \frac{\partial A^I_{Eik}}{\partial U_l}C^I_{Ekj}\delta U_l$$

$$+ C^R_{Eik}\frac{\partial A^R_{Ejk}}{\partial U_l}\delta U_l - C^I_{Eik}\frac{\partial A^I_{Ejk}}{\partial U_l}\delta U_l, \quad (17a)$$

$$\frac{d\delta C^I_{ij}}{dt} = A^R_{Eik}\delta C^I_{kj} + A^I_{Eik}\delta C^R_{kj} + \delta C^R_{ik}A^I_{Ejk} + \delta C^I_{ik}A^R_{Ejk}$$

$$+ \frac{\partial A^R_{Eik}}{\partial U_l}C^I_{Ekj}\delta U_l + \frac{\partial A^I_{Eik}}{\partial U_l}C^R_{Ekj}\delta U_l$$

$$+ C^R_{Eik}\frac{\partial A^I_{Ejk}}{\partial U_l}\delta U_l + C^I_{Eik}\frac{\partial A^R_{Ejk}}{\partial U_l}\delta U_l, \quad (17b)$$

$$\frac{d\delta U_i}{dt} = \frac{\partial\overline{vq}_{E,i}}{\partial C^R_{kl}}\delta C^R_{kl} + \frac{\partial\overline{vq}_{E,i}}{\partial C^I_{kl}}\delta C^I_{kl} - r_e\delta U_i, \quad (17c)$$

where $\mathbf{A}^R_E$ and $\mathbf{A}^I_E$ are the real and imaginary parts of the linear operator obtained by linearizing about the equilibrium mean flow $U_E(y)$ and the derivatives of the vorticity flux have been calculated about the equilibrium $(U_E, \mathbf{C}_E)$. The perturbation equations (17a)–(17c) may be written as

$$\frac{d}{dt}\begin{pmatrix} \delta\mathbf{C}^R \\ \delta\mathbf{C}^I \\ \delta U \end{pmatrix} = \mathbf{L}\begin{pmatrix} \delta\mathbf{C}^R \\ \delta\mathbf{C}^I \\ \delta U \end{pmatrix}, \quad (18)$$

with $\mathbf{L}$ a linear operator. Eigenanalysis of $\mathbf{L}$ determines the stability of the coupled equilibria.

In the adiabatic limit perturbations to the velocity profile, U, determine $\mathbf{C}$ uniquely through the asymptotic covariance equations $\mathbf{A}(U)\mathbf{C} + \mathbf{CA}^{\dagger}(U) = -\mathbf{Q}$, which is assumed to be satisfied at all times, and the stability of equilibrium U_E is then determined from Eq. (17c) in which the covariance perturbations have been expressed in terms of the velocity perturbations. The stability equation is only in U and has the form

$$\frac{d\delta U_i}{dt} = \frac{\partial\overline{vq}_{E,i}}{\partial U_j}\delta U_j - r_e\delta U_i. \quad (19)$$

This equation governing the stability of the equilibria in the adiabatic limit can be written symbolically as

$$\frac{d\delta U}{dt} = \mathbf{L}_{\mathrm{ad}}\delta U. \quad (20)$$

While the equilibria are the same for the fully coupled system (14a), (14b) and its adiabatic version (15a), (15b), the stability of the equilibria governed by $\mathbf{L}$ and $\mathbf{L}_{\mathrm{ad}}$ and the evolution of the mean velocity perturbation δU differ in the two cases.

The same variational equations can be used to study the stability of the trajectory of the coupled system of equations. When there are no stable equilibria, the stability of the solution trajectory $\mathbf{C}(t)$, $U(y, t)$ is found by calculating the Lyapunov exponent from the time-dependent variational equations (17a)–(17c) with the derivatives evaluated on the trajectory.

Remarks:

1) The traditional concept of jet stability addresses the stability of eddy perturbations assuming a jet structure. Stability in this sense is determined by the eigenvalue of the operator $\mathbf{A}$ with greatest real part. An equilibrium mean flow obtained by solving the adiabatic system (16) is by necessity stable in this sense because $\mathbf{A}(U_E)$ solves the Lyapunov equation $\mathbf{A}(U_E)\mathbf{C}_E + \mathbf{C}_E\mathbf{A}^{\dagger}(U_e) = -\mathbf{Q}$ with $\mathbf{C}_E$ positive definite (Brockett 1970). However, the time-dependent system (14a), (14b) allows for excursions of U that are transiently unstable and such intervals of instability are observed in examples. A second concept of jet stability was introduced in this section and it addresses the stability of the jet as an equilibrium structure maintained by the balance of eddy flux divergence and relaxation to the equilibrium flow, which would occur in the absence of eddies. Stability in this sense is determined by the real part of the eigenvalues of the coupled operator $\mathbf{L}$ (or its adiabatic variant $\mathbf{L}_{\mathrm{ad}}$).

2) The eigenfunctions of the $\mathbf{L}$ operator must be realizable, by which is meant that the perturbation co-

variance part of the eigenfunction must be Hermitian and the jet velocity part must be real. Because eigenvalues of **L** may occur in conjugate pairs, if an eigenvalue is complex the associated realizable functions are proportional to the sum or differences of the eigenfunctions associated with the pair of conjugate eigenvalues. Note that there is no requirement for the perturbation covariance to be positive definite (cf. Farrell and Ioannou 2002).

4. Examples of wave–mean flow equilibria

a. Formulation of the wave–mean flow system for a barotropic jet

As an example consider the equivalent barotropic dynamics of a zonal flow on a midlatitude β plane. This example models vacillation of the upper-tropospheric zonal jet due to eddy momentum-flux divergence (Lee and Feldstein 1996; Robinson 1996; Hartmann and Lo 1998; Lorenz and Hartmann 2001; Watterson 2002; Koo et al. 2002). The perturbation dynamics obey the forced linear equation

$$\frac{d\hat{\psi}}{dt} = \mathbf{A}(U)\hat{\psi} + \mathbf{F}\xi(t), \qquad (21)$$

with

$$\mathbf{A}(U) = (D^2)^{-1}\left\{-ikU(y, t)D^2 - ik\left[\beta - \frac{d^2U(y, t)}{dy^2}\right]\right\}$$

$$- r\mathbf{I} - (D^2)^{-1}\left(\frac{dr}{dy}\frac{d}{dy}\right), \qquad (22)$$

where

$$D^2 \equiv \frac{d^2}{dy^2} - k^2 - l^2, \qquad (23)$$

k is the zonal wavenumber, y is the meridional coordinate, l^2 is the Froude number, and r is a coefficient of Rayleigh friction. The equations are written in dimensionless form using length $L = 2820$ km and velocity $U_0 = 30$ m s^{-1}, so that the unit of time is $L/U_0 = 1.1$ day. The corresponding nondimensional midlatitude value for the planetary vorticity gradient is $\beta = 4.264$ and waves with zonal wavenumber $k = 5$ correspond to zonal wavenumber 8 at latitude 45°.

Assume a single nonzero column in the forcing structure matrix **F** and take it to be proportional to the radiative equilibrium flow $U_e(y)$. This stochastic forcing models the baroclinic processes that are not represented in our equivalent barotropic dynamics but that are expected to produce forcing concentrated in the region of the jet. The results that we report do not depend qualitatively on the chosen forcing structure assuming that the jet core is forced stochastically. In most calculations to follow we assume that the nondimensional trace of the forcing covariance is trace(**Q**) = 0.0125, which cor-

responds to a kinetic energy injection rate of 1.2×10^{-4} W kg^{-1}. Such an injection rate induces jet accelerations of the order of 0.5 m s^{-1} day^{-1} averaged over the whole channel and approximately 1 m s^{-1} day^{-1} over the region of the jet maximum.

Take the radiative equilibrium velocity profile

$$U_e = \frac{1 + \cos[\pi(y - 1)]}{2}, \qquad (24)$$

and confine the flow to a meridional channel on $0 \leq y \leq 2$, with boundary condition $\hat{\psi} = 0$ at $y = 0, 2$. Adjacent to the boundaries introduce sponge layers with the Rayleigh friction coefficient

$$r_s(y) = 2\left\{\left[1 - \frac{\tanh(y - 0.3)}{0.1}\right]\right.$$

$$\left. + \left[1 + \frac{\tanh(y - 1.7)}{0.1}\right]\right\}, \qquad (25)$$

in order to enforce radiation boundary conditions.

b. Structural stability of the coupled barotropic jet system

Consider first the structure of the jet equilibria as a function of the strength of the eddy forcing. For simplicity take the perturbation structure to be concentrated in the single zonal wavenumber $k = 6$ and the eddy forcing to be given by $\epsilon\mathbf{Q}$ with trace(**Q**) = 0.0125 (so that realistic atmospheric forcing corresponds to $\epsilon \approx 1$). The results are shown in Fig. 1. For small forcing, ϵ, there is a single stable symmetric equilibrium. As the forcing increases the stability of this symmetric equilibrium decreases and it becomes neutral at $\epsilon \approx 0.1$ where both the real and imaginary parts of the least-stable eigenvalue of the matrix **L** of the coupled system (18) vanish. By necessity at this value of ϵ the stability of the symmetric equilibrium is also lost in the adiabatic perturbation dynamics governed by $\mathbf{L}_{ad}$. As ϵ is further increased the symmetric equilibrium eventually becomes unstable and at the point of neutrality there is a supercritical pitchfork bifurcation giving rise to two stable asymmetric states. In the specific case in which the forcing is symmetric these asymmetric states are mirror images[1] with respect to the center of the channel at $y = 1$ (Fig. 2).

---

[1] This mirror image symmetry can be generalized: if the radiative equilibrium flow U_e is symmetric and the forcing **F** is either symmetric or proportional to the instantaneous mean flow, then asymmetric equilibrium velocities $U_E(y)$ exist in pairs. To see this consider the channel to be centered at $y = 0$. If the time-independent flow $U_E(y)$ is an equilibrium solution of the coupled system then so is the reflected flow $U_E(-y)$. Because for forcing **F** that are either symmetric about the channel center ($y = 0$) or proportional to the mean velocity $U_E(y)$ the perturbations $\hat{\psi}(y)$ that arise with mean flow $U_E(y)$ are identical with the perturbations $\hat{\psi}(-y)$ that arise with mean flow $U_E(-y)$, so that the equilibrium condition $\overline{vq}_E = r_e(U_E - U_e)$, is satisfied both for $U_E(y)$ and $U_E(-y)$.
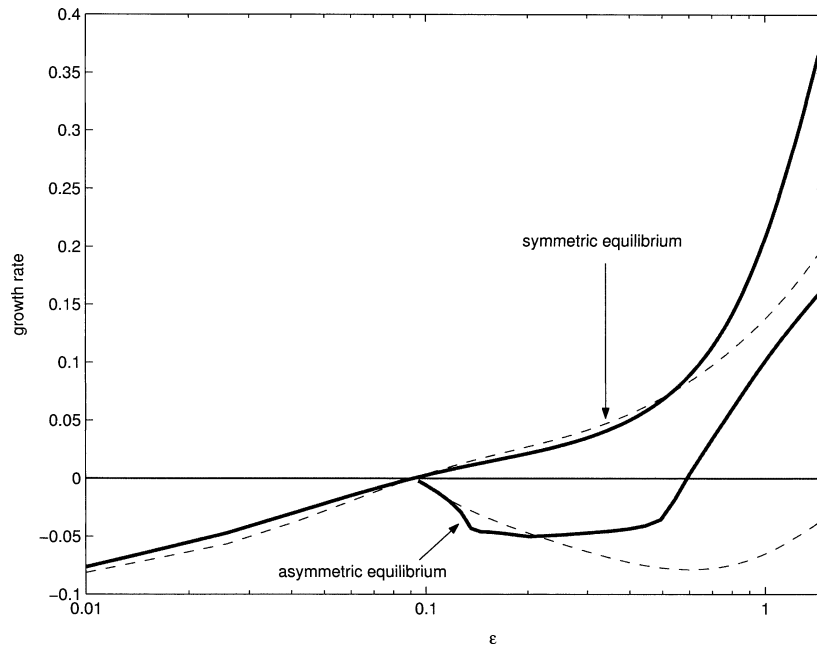
FIG. 1. Maximum growth rate of perturbations to the equilibrium structure of the barotropic jet as a function of the strength of the forcing measured by ϵ trace($\mathbf{Q}$). The continuous curves are the growth rates of perturbations to the symmetric and asymmetric equilibria (i.e., the max real part of the eigenvalues of $\mathbf{L}$). The dashed lines are the corresponding growth rates in the adiabatic approximation (i.e., the max real part of the eigenvalues of $\mathbf{L}_{ad}$). The parameters are $k = 6$, $r = 0.05$, $r_e = 0.1$, $l = \pi$; 21 levels have been used for the calculation of the equilibria and their respective stability, trace($\mathbf{Q}$) = 0.0125 and $\beta =$ 4.264. A single structure in the shape of the symmetric radiative equilibrium flow (24) is stochastically forced.

With still further increase of ϵ the asymmetric equilibria become neutrally stable at $\epsilon_h \approx 0.6$, where $\mathbf{L}$ has a pair of imaginary eigenvalues, no other eigenvalues with zero real parts exist, and the real part of the eigenvalues is increasing with ϵ in the neighborhood of ϵ_h. Therefore, at this point a supercritical Hopf bifurcation gives rise to a stable limit cycle associated with a periodic vacillation of the mean flow (Fig. 3). Note that if the dynamics are limited to the adiabatic approximation (dashed line in Fig. 1) the asymmetric equi-
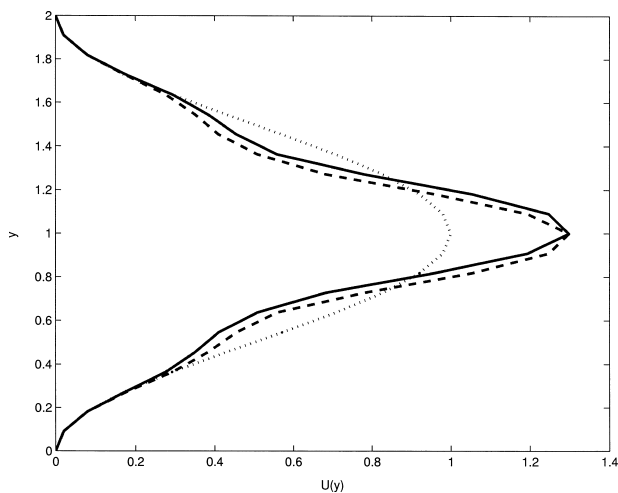

FIG. 2. The unstable asymmetric equilibria of the barotropic jet for stochastic forcing with magnitude $\epsilon = 1.5$ (solid and dashed lines) and the radiative equilibrium flow (dotted line). The parameters are the same as in Fig. 1.
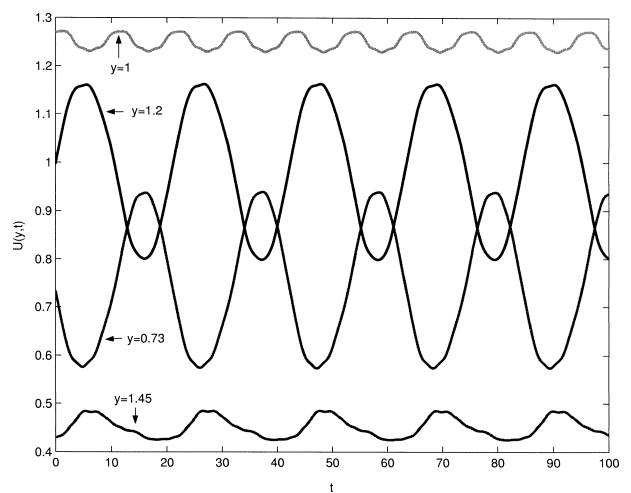

FIG. 3. Time series of the mean flow velocity for the barotropic jet at the locations indicated on the graph. The stochastic forcing has magnitude $\epsilon = 1$. The mean flow is in a limit cycle. The other parameters are the same as in Fig. 1.
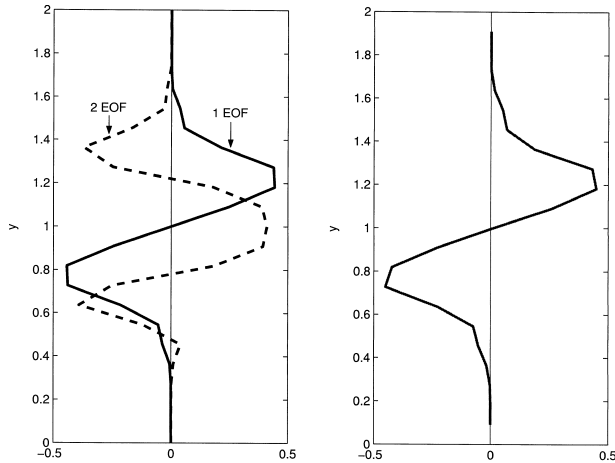
FIG. 4. (left) The first two EOFs of the mean velocity fluctuation in the barotropic jet. The first EOF (continuous line) is antisymmetric and explains nearly all the mean flow variance (97%), while the second (dashed line) is symmetric and explains 2% of the variance. (right) The real part of the velocity of the most unstable eigenfunction of the operator $\mathbf{L}$ that determines the stability of perturbations about the asymmetric equilibrium. The corresponding eigenvalue is $0.1 + i0.2$. Note that the structure of the most unstable velocity perturbation is the same structure as the dominant EOF. The stochastic forcing has magnitude $\epsilon = 1$. The mean flow is in a limit cycle, the zonal wavenumber is $k = 6$. The parameters are the same as in Fig. 1.

libria remain stable and no vacillation occurs, implying that coupling of the time-dependent forms of the wave–mean flow equations are required for limit cycle behavior. The first two EOF's of the mean wind variation are shown in Fig. 4 (left). The first EOF is antisymmetric and is nearly the same as the equivalent barotropic dipole structure obtained by Lorenz and Hartman (2001) in their study of Southern Hemisphere midlatitude jet vacillation. Figure 4 (right) shows the real part of the velocity perturbation of the most unstable eigenfunction of the operator $\mathbf{L}$ governing perturbations about the unstable asymmetric equilibrium. This unstable velocity structure governs the breakdown of the asymmetric equilibrium, which equilibrates into a limit cycle of the zonal wind with dominant EOF of mean wind variations very similar to the structure of the unstable eigenfunction. The period of the limit cycle at $\epsilon = 1$ is smaller than that predicted from the period of oscillation of the most unstable mode of operator $\mathbf{L}$, but for parameter values near the bifurcation $\epsilon_h \approx 0.6$ the period of the limit cycle is given by the period of the most unstable eigenfunction. This limit cycle behavior persists up to $\epsilon \approx 5$ at which point the limit cycle becomes unstable and the vacillation becomes chaotic through period doubling. All of these results have been verified by simulations at high resolution.

The essence of jet vacillation dynamics has been captured by this simple model. However, there are two issues that we wish to investigate further: the first is that observed vacillation is not purely periodic and the second is that the variance explained by the first EOF in

observations, while dominant, is not 97% as we have found when the system is in the limit cycle regime. It is tempting to take the irregularity of the jet vacillation as an indication that the jet is in the chaotic regime. But we believe that this is unlikely because the physical parameters that correspond to the chaotic regime are not realistic (very strong forcing, and high wavenumber perturbations). It could also be argued that exact periodicity and dominance of a single EOF are due to the simplicity of the model. However, we will show in the next section that these features of the jet vacillation have a more fundamental explanation and that terrestrial jet dynamics rather than being in the limit cycle regime is more likely to be in the multiple equilibria regime, which in the asymptotic dynamics exhibits two asymmetric equilibria.

Similar bifurcation properties are revealed when we use the eddy zonal wavenumber, k, as the bifurcation parameter rather than the stochastic forcing magnitude ϵ. In these experiments $\epsilon = 1$, which is appropriate for atmospheric forcing. The bifurcation diagram is shown in Fig. 5. For wavenumbers smaller than $k \approx 4$ (corresponding to global zonal wavenumber 6) there is a single stable symmetric equilibrium, which gives rise to two asymmetric equilibria through a supercritical pitchfork bifurcation. The asymmetric states then undergo a supercritical Hopf bifurcation at $k \approx 5.2$ (dimensional zonal wavenumber 8) at which point the jet structure assumes stable limit cycle behavior. For larger wavenumbers the trajectory becomes chaotic. The transition from stable limit cycle behavior to chaos is shown in Fig. 6. While single wavenumber forcing is physically idealistic the qualitative character of this diagram persists in multiwave experiments with peaked k spectra.

The influence of the radiative equilibrium flow magnitude and structure μU_e is shown as a function of μ for zonal wavenumber $k = 4$ waves in Fig. 7. At $k = 4$ and $\mu = 1$ a single stable symmetric equilibrium is obtained, which is shown in Fig. 8 (right). As μ is reduced this symmetric equilibrium becomes unstable and two stable asymmetric equilibria appear; these remain stable up to $\mu = 0$. The equilibria for $\mu = 0$ are shown in Fig. 8 (left). These stable asymmetric equilibria for $\mu = 0$ are remarkably robust persisting over a wide range of wavenumbers, forcings, and dissipation parameters. The only parameter found to break the stability of the asymmetric states is $\beta = 0$ for which limit cycle or even chaotic solutions exist.

Remarkably, linear stability of the equilibria is almost always indicative of global nonlinear stability, the only exceptions found were for cases with $U_e = 0$ or with $\beta = 0$. In these cases linear stability has a finite radius of validity around the equilibrium solution.

c. Formation and maintenance of multiple jets

Existence of equilibria even in the absence of a radiative equilibrium jet has implications for the atmo-
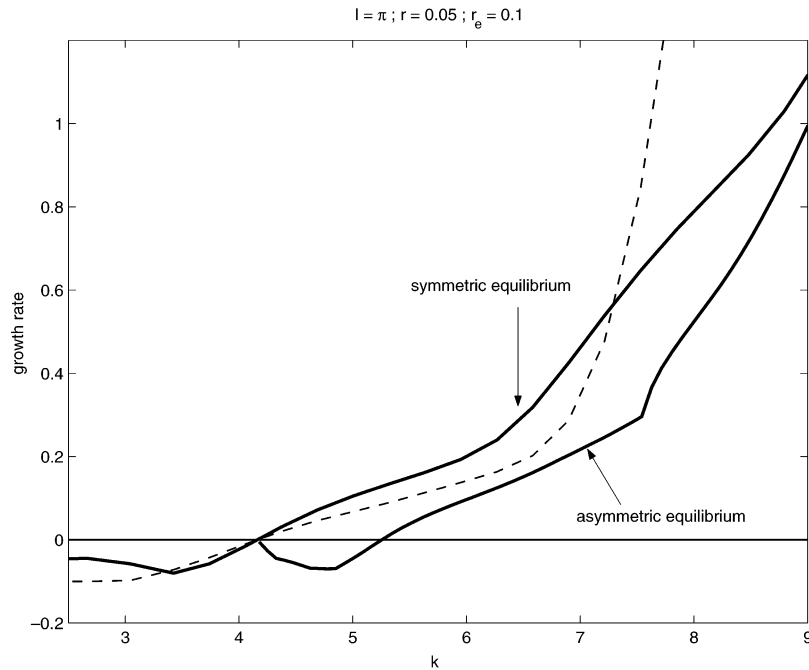
$l = \pi$; $r = 0.05$; $r_e = 0.1$

FIG. 5. Maximum growth rate of perturbations to the symmetric and asymmetric equilibria as a function of zonal wavenumber k. Continuous lines are the maximum growth rate of perturbations to the symmetric equilibrium and the asymmetric equilibria from eigenanalysis of $\mathbf{L}$; dashed lines are the maximum growth rate of perturbations to the symmetric equilibrium obtained from the adiabatic operator $\mathbf{L}_{\mathrm{ad}}$. [The parameters are $r = 0.05$, $r_e = 0.1$, $l = \pi$; 21 levels have been used for the calculation of the equilibria and their respective stability, and the forcing has $\epsilon = 1$ and $\beta = 4.264$. A single structure in the shape of the symmetric radiative equilibrium flow (24) is stochastically forced.]
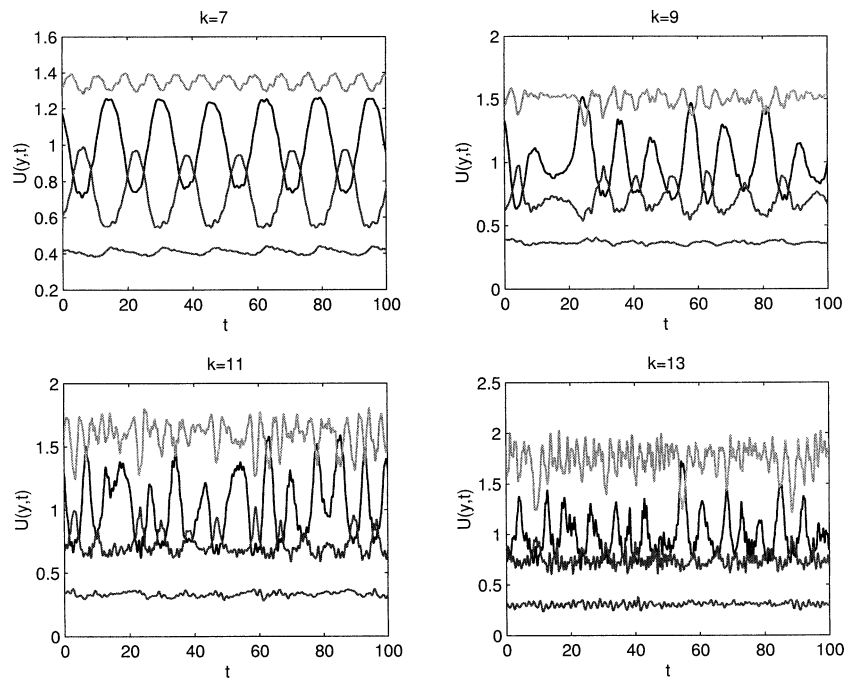

FIG. 6. The mean flow velocity in the barotropic problem at four meridional locations $y = 1.45, 0.73, 1.2, 1$ as in Fig. 3. The panels are for $k = 7, 9, 11, 13$. The other parameters are as in Fig. 5. This figure demonstrates transition from a stable limit cycle to chaos as the wavenumber of the forcing increases.
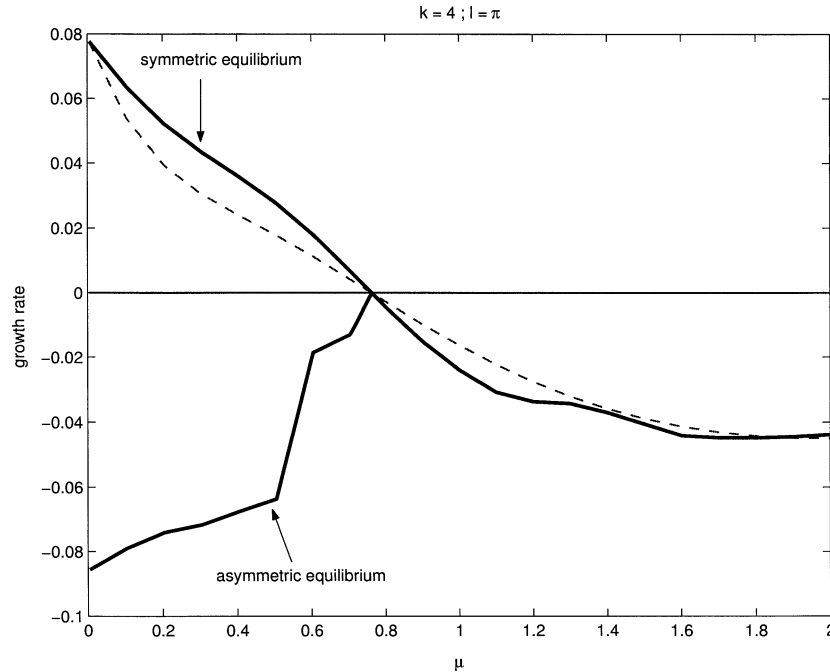
FIG. 7. Maximum growth rate of perturbations to the symmetric and asymmetric equilibria of the barotropic model as a function of the magnitude of the radiative equilibrium flow μ. Continuous lines are the maximum growth rate of perturbations to the symmetric equilibrium and the asymmetric equilibria from eigenanalysis of the operator $\mathbf{L}$ of coupled system (18); dashed line is maximum perturbation growth rate from the adiabatic $\mathbf{L}_{ad}$ operator (20) for the symmetric equilibrium. (The parameters are $r = 0.05$, $r_e = 0.1$, $k = 4$, $l = \pi$; 21 levels have been used for the calculation of the equilibria and their respective stability, and the forcing has trace($\mathbf{Q}$) = 0.0125 and $\beta = 4.264$. A single structure in the shape of the symmetric radiative equilibrium flow (24) is stochastically forced.)
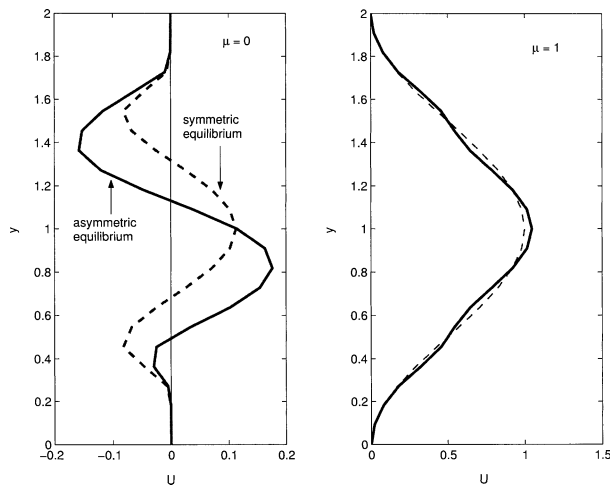

FIG. 8. (left) The symmetric (dashed line) and asymmetric equilibrium (continuous line) flow for the barotropic model with stochastic forcing but without a radiative equilibrium flow ($\mu = 0$). The symmetric equilibrium is unstable, while the asymmetric equilibria are stable (there is another asymmetric flow equilibrium that is the mirror image with respect to the center of the channel). The stability properties of these equilibria are shown in Fig. 7. (right) The symmetric equilibrium (continuous line) for the radiative flow U_e (dotted line; $\mu = 1$), given by (24). The symmetric equilibrium is stable. There are no other equilibria in this case. The other parameters are as in Fig. 7.

spheres of the outer planets, which are characterized by multiple jets with meridional scale unrelated to radiative forcing scale. With $U_e = 0$ we find stable equilibria with multiple jets in the asymptotic large-ensemble limit. An example for terrestrial parameters is shown in Fig. 9. The number of jets is not determined by the structure of the forcing. In the example, four forcing harmonics were used but an equilibrium jet with the same number of jets is maintained even with a single forcing, which is constant in y while varying in time as a white noise process. Multiple jets with the same number of jet maxima were also found with $\beta = 0$.

d. Abrupt reorganization of the equilibrium jet when it is subject to small changes in the equivalent radiative equilibrium forcing

The ice core climate record suggests that rapid reconfiguration of jet statistics occurs on timescales short compared to orbital parameter variation and ice sheet dynamics (Dansgaard et al. 1993). A possible explanation for this phenomenon is reconfiguration of jet equilibria when a threshold forcing is passed in the radiative equilibrium forcing maintaining the jet.

In order to study this phenomenon we slowly vary the equivalent radiative equilibrium profile in the bar-
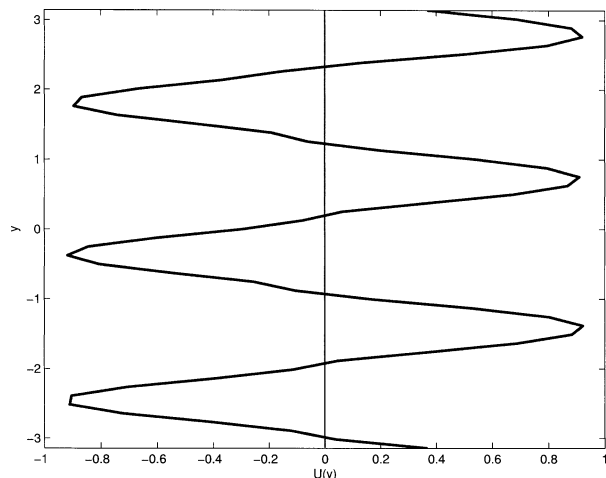
FIG. 9. A multiple jet equilibrium velocity profile. There is no equilibrium velocity profile being relaxed to. The channel extent in y is $[-\pi, \pi]$ corresponding to 18 000 km and it is reentrant in this direction. Ensemble mean forcing was used with covariance $\mathbf{Q} = \alpha \sum_{k=1}^{4} \sin ky (\sin ky)^{\dagger} + \cos ky (\cos ky)^{\dagger}$, where the coefficient α has been chosen so that $\text{trace}(\mathbf{Q}) = 0.0125$. The other parameters are $r = 0.25$, $r_e = 0.1$, $l = 0$, $\beta = 4.264$ and $k = 5$.

otropic model of the jet dynamics, presented in the previous section, by moving the center of the radiative equilibrium profile (24) poleward as a model of radiation modulation as a result of slow retreat of the equa-torward margin of the glaciers and/or orbital parameter modulated distribution of radiative forcing.

We find two jet equilibria exist for equivalent radiative equilibrium forcing centered at $y = 1$ (Fig. 10a). These equilibria represent the subtropical and polar jet in the model. A very slight poleward displacement in the position of the radiative equilibrium jet to $y = 1.05$ results in disappearance of the subtropical jet while the polar jet is only slightly modified from its structure when the forcing was centered at $y = 1$ (Fig. 10b). This rearrangement of the jets occurs because the subtropical jet becomes unstable in the coupled wave–mean flow equations indicating that eddy flux can not maintain the southerly jet. This instability of the subtropical jet occurs when the center of the radiative forcing has moved to $y = 1.045$. This loss of the subtropical jet occurs as a threshold is passed in the radiative forcing.

e. An example of vacillation in a stratified flow, the QBO

Consider a stratified zonal flow $U(z, t)$ interacting with eddies where z is now the vertical direction. The linearized equation for harmonic perturbations in streamfunction $\hat{\psi}(z, t)e^{ikx}$ and density $\hat{\rho}(z, t)e^{ikx}$ are

$$\frac{d}{dt}\begin{pmatrix} \hat{\psi} \\ \hat{\rho} \end{pmatrix} = \mathbf{A}(U)\begin{pmatrix} \hat{\psi} \\ \hat{\rho} \end{pmatrix} + \mathbf{F}\xi(t), \qquad (26)$$

with linear operator

$$\mathbf{A}(U) = \begin{bmatrix} (D^2)^{-1}(-ikUD^2 + ikU'' - r'd/dy) - r\mathbf{I} & -ik\,\text{Ri}(D^2)^{-1} \\ ik & -ik\mathbf{I} - r\mathbf{I} \end{bmatrix}, \qquad (27)$$

where $'$ denotes differentiation in z and

$$D^2 \equiv \frac{d^2}{dz^2} - k^2. \qquad (28)$$

We have neglected the Coriolis acceleration, made the Boussinesq approximation, and assumed a constant Brunt–Väisälä frequency with stratospheric value $N_0 = 2 \times 10^{-2}\ s^{-1}$. With length scale $L = 15.8$ km and velocity scale $U_0 = 10$ m s^{-1}, the unit of time is $L/U_0 = 25$ min (so that a day is 55 nondimensional units, and a year is 20 000 units). The Richardson number is $\text{Ri} = N_0^2 L^2/U_0^2 = 10^3$ and a Rayleigh damping distribution $r = 10^{-3}(1 + e^z)$ models increased thermal damping in the upper atmosphere. The chosen Rayleigh damping gives decay time of 18 days at the channel base. Waves with zonal wavenumber $k = 2$ are taken corresponding to a 50-km dimensional wavelength. A single nonzero column in the forcing structure matrix $\mathbf{F}$ excites only the streamfunction part of the perturbation proportionally to e^{-z} with an additional taper at the channel end. This $\mathbf{F}$ models gravity wave forcing maximizing in the lower stratosphere.

The evolution equation for the mean is

$$\frac{dU}{dt} = \overline{vq} - r_e U, \qquad (29)$$

with $\hat{q} = D^2\hat{\psi}$ and radiative relaxation coefficient $r_e = 10^{-4}$ giving a relaxation time back to the equilibrium zero velocity profile of 182 days.

The flow is confined in the vertical to $0 \le z \le 2$, with boundary condition $\hat{\psi} = 0$ and $\hat{\rho} = 0$ at $z = 0, 2$. Adjacent to the boundaries sponge layers of the shape used in the barotropic example enforce radiation boundary conditions.

The resulting limit cycle behavior for gravity waves with $k = 2$ and stochastic forcing amplitude $\text{trace}(\mathbf{Q}) = 0.125$ is shown as a Hoevmöller diagram in height and time in Fig. 11. The ensemble mean equations clearly capture the primary features of the QBO including the long timescale and the downward phase propagation of the zonal velocity.
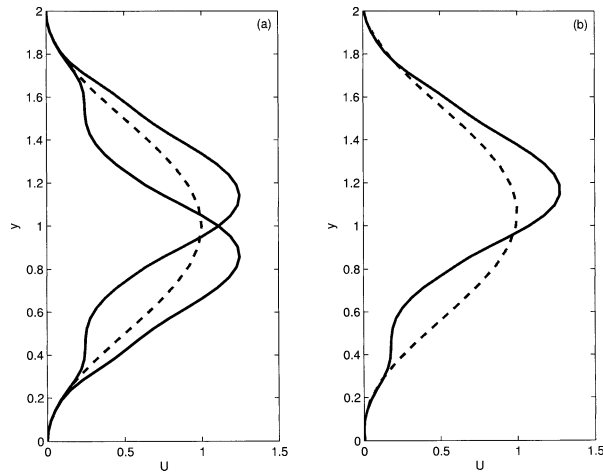
FIG. 10. (a) Two equilibrium zonal jets (continuous lines) are supported by the indicated equivalent radiative equilibrium profile (dashed line) to which the flow is being relaxed to. The maximum of the radiative equilibrium flow is at the center of the channel ($y = 1$). Both zonal jets are stable equilibria of the wave–mean coupled equations. (b) The single remaining equilibrium jet when the radiative equilibrium maximum is shifted to $y = 1.05$ (dashed line). The southern jet, which existed as a stable equilibrium when the radiative equilibrium flow was centered at $y = 1$ becomes unstable when the radiative equilibrium jet maximum shifts to $y = 1.045$. Ensemble mean forcing is the same as that used in Fig. 5 (but because 41 levels were used in these integrations the trace had to be taken as trace($\mathbf{Q}$) = 2×0.0125). The other parameters are $r = 0.25$, $r_e = 0.05$, $l = \pi$, $\beta = 4.264$ and $k = 5$.

5. Modification of the asymptotic solution resulting from assuming a finite number of forcing structures in the ensemble

We have investigated the dynamics of the coupled mean equations (14a), (14b) and found that this autonomous system has an orderly behavior with the mean flow equilibrating to a steady jet, vacillating periodically, or being chaotic. As discussed earlier, the ensemble mean dynamic equations are an accurate approximation of wave–mean flow interaction only if an adequate number of independent ensemble members are present around a latitude circle. This requires the autocorrelation length of the forcing be small compared to the length of the latitude circle. In some physical situations this requirement is fulfilled: if the QBO is forced by tropospherically excited gravity waves of scale 10–1000 km (Dunkerton 1997), then the mean flow is forced by 40–4000 independent ensemble members; if the solar cycle is forced by the convective motions of the supergranules of scale 3.5×10^4 km there are about 100 ensemble members in the solar equator; if the Jovian mean winds are forced by convection on 1000-km scale then the mean flow is forced by 300 independent ensemble members. In all these cases ensemble mean dynamics is valid for the mean flow. However, there are cases for which the infinite ensemble limit may be questionable; for example, in the terrestrial midlatitudes the autocorrelation length of the mean flow is the cyclone scale of $\approx$3000 km, so that the mean flow is forced by $O(10)$ independent ensemble members. This raises the question of how the infinite ensemble results
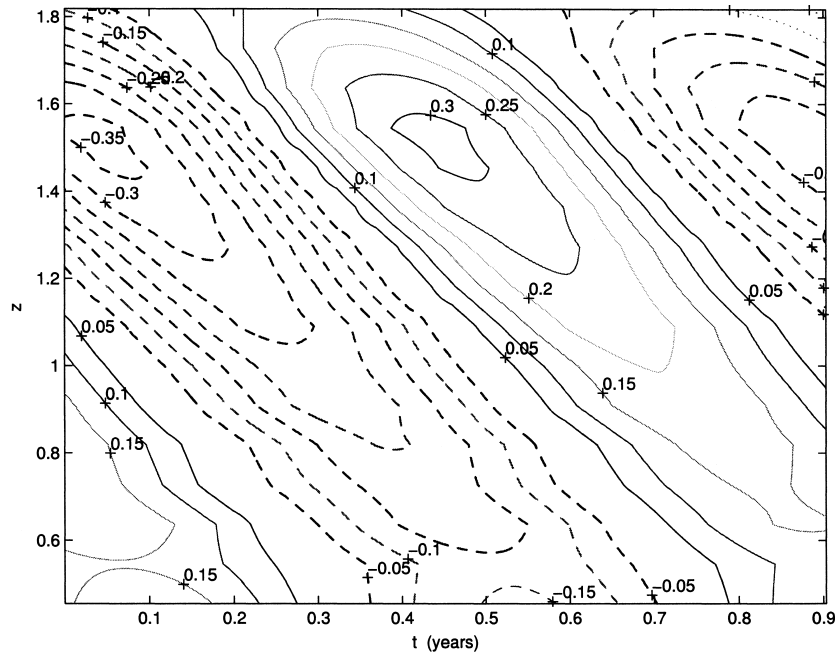

FIG. 11. Hovmöller diagram of the limit cycle behavior in stratified flow. The ensemble mean equations are forced only with waves with zonal wavenumber $k = 2$, and the Richardson number is Ri = 10^3. The amplitude of the stochastic forcing is trace($\mathbf{Q}$) = 0.125.
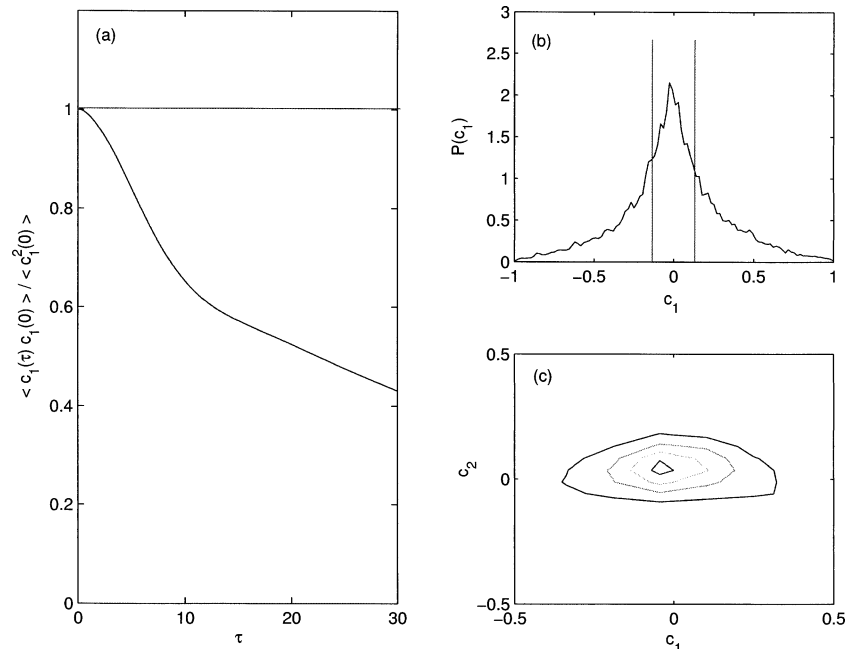
FIG. 12. (a) The autocorrelation of the first principal component of the jet fluctuations, c_1, as a function of delay time, τ, for the case in which the jet is forced by five ensemble members. At the top of the graph is shown the autocorrelation of the equilibrium jet with ensemble mean forcing when the jet is at one of its equilibrium configurations. (b) The probability density function of the first principal component for the case of stochastic forcing by five ensemble members and the pdf for ensemble mean forcing (the two delta functions). (c) The pdf of the first two principal components for the forcing by five ensemble members. The perturbations have zonal wavenumber $k = 5$, the stochastic forcing has trace($\mathbf{Q}$) = 0.0125 and the other parameters are as in Fig. 5.

presented in the previous section are approached as the number of ensemble members increases, and how many ensemble members are required for the ensemble mean dynamics to emerge.

Consider the behavior of the mean jet in the barotropic example with $l = \pi$, stochastic forcing with $\epsilon = 1$, and other parameters as in the previous section and examine the two cases of $k = 5$ and $k = 6$. From the bifurcation diagram for the ensemble mean dynamics shown in Fig. 5 we see that at wavenumber 5 (corresponding to zonal wavenumber 8 at 45° latitude) the jet equilibrates to one of the two possible equilibria, while at wavenumber 6 the mean jet vacillates in a limit cycle.

Let us first consider the $k = 5$ case. For an infinite number of forcing ensemble members the jet dynamics is governed by the ensemble mean equations and therefore equilibrates to one of the two available equilibria. Assuming that there is no bias this could be either U_{eq}^+ or U_{eq}^-. Given that with equal probability the state of the jet is either U_{eq}^+ or U_{eq}^- the only EOF describing the two equilibria is

$$U_{\text{EOF}} = \frac{U_{eq}^+ - U_{eq}^-}{\|U_{eq}^+ - U_{eq}^-\|},\qquad(30)$$

(with $\|\cdot\|$ the Euclidean norm). In that case the probability density function (pdf) of the first principal com-

ponent, c_1, (the only nonzero principal component in that case) would be two delta functions centered at the projection of the two states $U_{eq}^\pm - (U_{eq}^+ + U_{eq}^-)/2$ on the U_{EOF}. This bimodal distribution is shown in Fig. 12b. These equilibria are infinitely persistent and the autocorrelation of the first principal component

$$\frac{\langle c_1(\tau)c_1(0)\rangle}{\langle c_1^2(0)\rangle}\qquad(31)$$

as a function of the delay, τ, is a straight line shown in Fig. 12a. The single EOF of these two equilibria (30) is shown in Fig. 13. We consider now the corresponding behavior of the jet when it is forced by a few ensemble members [cf. (8a)–(8c) or (9a), (9b)], as is appropriate for the midlatitude atmosphere, and for definiteness we force with five independent ensembles. Under such forcing the jet fluctuates in an irregular manner. Do these fluctuations show any scars of the multiple equilibria of the underlying ensemble average equations? The centered and unimodal but non-Gaussian probability density function (pdf) of the first principal component of the fluctuating jet, shown in Fig. 12b, is very different from the bimodal distribution that arises in the case of ensemble mean forcing. The pdf of the first two principal components, which is shown in Fig. 12c, is also centered and unimodal with no obvious relation to the
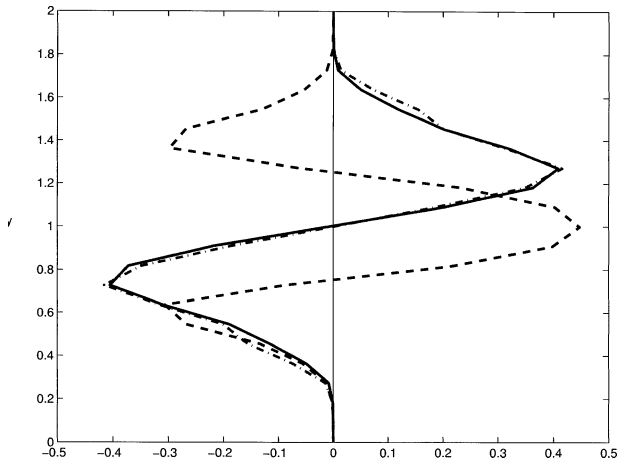
FIG. 13. The first two EOFs of the mean velocity fluctuation in the barotropic jet when the jet is stochastically forced by five ensemble members. The first EOF (continuous line) accounts for 85% of the mean flow variance, while the second (dashed line) is symmetric and explains 10% of the variance. This first EOF is almost identical with the EOF given by (30) corresponding to a switch between the two equilibria that exist for ensemble mean forcing (dash–dot line). The parameters are the same as those of Fig. 12.

corresponding bimodal pdf associated with the ensemble mean forcing. Similar pdf's arise in the observed fluctuations of the jet in the Southern Hemisphere (Koo et al. 2002). The autocorrelation of the first principal component shown in Fig. 12a shows persistence of approximately 15 days indicative of a red noise process. No periodicities are seen. The corresponding two dominant EOFs (which account for 85% and 10% of the fluctuation variance respectively are shown in Fig. 13. It is remarkable that the first EOF of the jet fluctuation for the five ensemble member case reproduces the EOF corresponding to switching between the two equilibria of the asymptotic ensemble averaged equations. Both the EOF structure and the autocorrelation of the first principal component are very close to those found from observations of jet fluctuations in the Southern Hemisphere (Lorenz and Hartmann 2001). These results suggest that the Southern Hemispheric jet is in the multiple equilibria regime to the left of the supercritical Hopf bifurcation in Fig. 5 but with too few ensemble members to reveal the bimodality of the underlying asymptotic dynamics.

Let us consider now the case of wavenumber $k = 6$ for which the asymptotic ensemble mean forcing leads to a periodic oscillation of the mean jet (cf. Fig. 3) with EOFs shown in Fig. 4. The probability density function of the first principal component shown in Fig. 14b reveals this oscillatory variation of the zonal jet structure. The pdf of the first two principal components, shown in Fig. 14b, is concentrated on the orbit with the density of states high in regions of the orbit in which the rapidity of variation of the corresponding principal components is small. The autocorrelation of the first principal component, shown in Fig. 14a, reveals the periodicity of

vacillation of the zonal jet. However, when the jet is forced by five ensemble members the pdf of the first principal component, shown in Fig. 15, while non-Gaussian is unimodal and similar to that obtained for the case of similar forcing of the regime in which the ensemble mean equations admitted multiple equilibria solutions (cf. Fig. 12). Nevertheless, the autocorrelation of the first principal component, shown in Fig. 15a, shows scars of the periodicity of the ensemble mean jet dynamics. While the autocorrelation shows scars of periodicity the EOFs are almost identical to the EOFs of the ensemble mean dynamics (cf. Fig. 4) and to the EOFs obtained from data. The periodicity revealed in the autocorrelation of the first principal component when the zonal jet is forced by five member ensembles in the limit cycle regime of the asymptotic system is not seen in data (cf. Lorenz and Hartmann 2001) which leads us to conclude that the terrestrial atmosphere most likely lies in the multiple equilibria regime before the Hopf bifurcation to limit cycle behavior in the asymptotic equations.

We demonstrate convergence to the ensemble mean solution as the number of members in the ensemble of forcings is increased using as an example convergence for perturbations with zonal wavenumber $k = 6$. As previously discussed, the ensemble mean dynamics corresponding to an infinite number of ensemble members results in limit cycle behavior. This is indicated in Fig. 16d where the power spectrum of the time series of the mean flow velocity at the center of the channel (latitude $y = 1$) is plotted as a function of frequency. The fundamental frequency associated with the limit cycle and its overtones are clearly seen. The spectral peak is still present when 64 members are included in the forcing (Fig. 16c) in which a time series of length of 1.5×10^4 time units was used to approximate the spectra (corresponding to about 1.5×10^3 periods of the limit cycle). However, the spectral peak is not present when only eight ensemble members are included in the forcing (Fig. 16b) and the spectrum with a single ensemble member is red (Fig. 16a). Recall, however, that while the spectrum of the complete U variation is red, analysis of the temporal variation of the first principal component does reveal an indication of imperfect recurrence that can be traced to the perfect periodicity of the underlying limit cycle identified in the ensemble mean dynamics.

6. Conclusions

Organization of coherent jets by turbulent eddy fields is commonly observed in both rotating and nonrotating fluids. We have presented a comprehensive theory for this phenomenon building on results from linear stochastic turbulence theory, which allow calculation of the eddy covariance in statistical equilibrium with a given turbulent jet. Coupling the eddy forcing arising from the jet–turbulence interaction obtained from this theory with the evolution for the zonal jet produces a set of
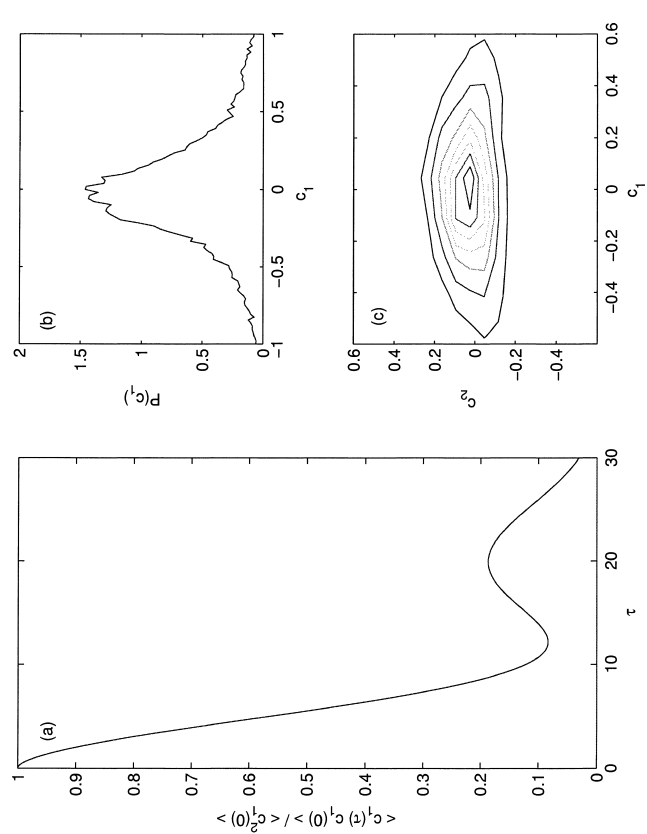
FIG. 15. (a) The autocorrelation of the first principal component of the jet fluctuations, c_1, as a function of delay time, τ, for the case in which the jet is forced by five ensemble members. A scar of the periodic behavior that occurs for forcing with infinite ensemble members is discernible. (b) The probability density function (pdf) of the first principal component for the forcing by five ensemble members. (c) The pdf of the first two principal components for the forcing by five ensemble members. The perturbations have zonal wavenumber $k = 6$, the stochastic forcing has trace($\mathbf{Q}$) $= 0.0125$ and the other parameters are as in Fig. 5.
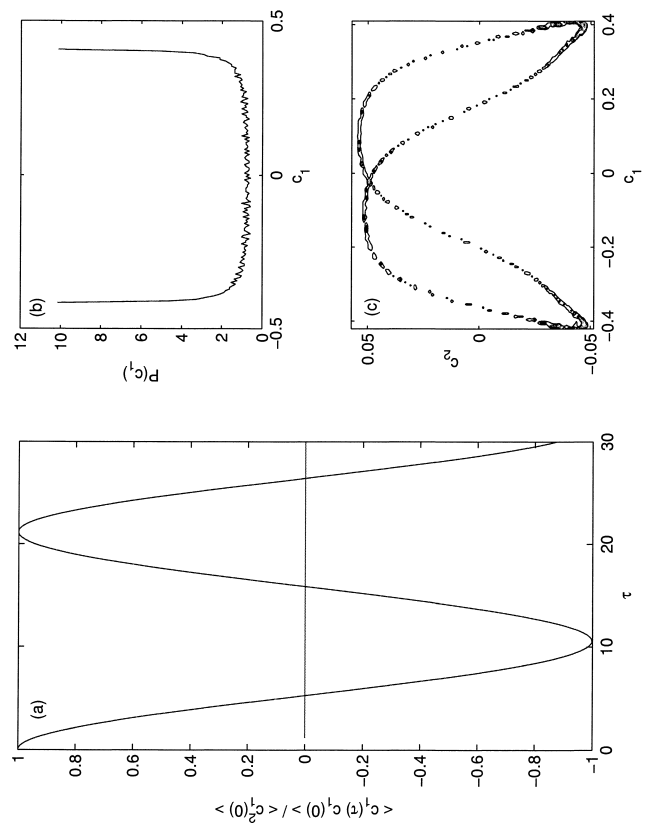

FIG. 14. (a) The autocorrelation of the first principal component of the jet fluctuations, c_1, as a function of delay time, τ, for the case in which the jet is forced by the ensemble mean stochastic forcing. The jet fluctuates periodically. (b) The probability density function of the first principal component for ensemble mean forcing. (c) The pdf of the first two principal components for ensemble mean forcing. The two principal components traverse a Lissajous figure. The perturbations have zonal wavenumber $k = 6$, the stochastic forcing has trace($\mathbf{Q}$) $= 0.0125$ and the other parameters are as in Fig. 5.
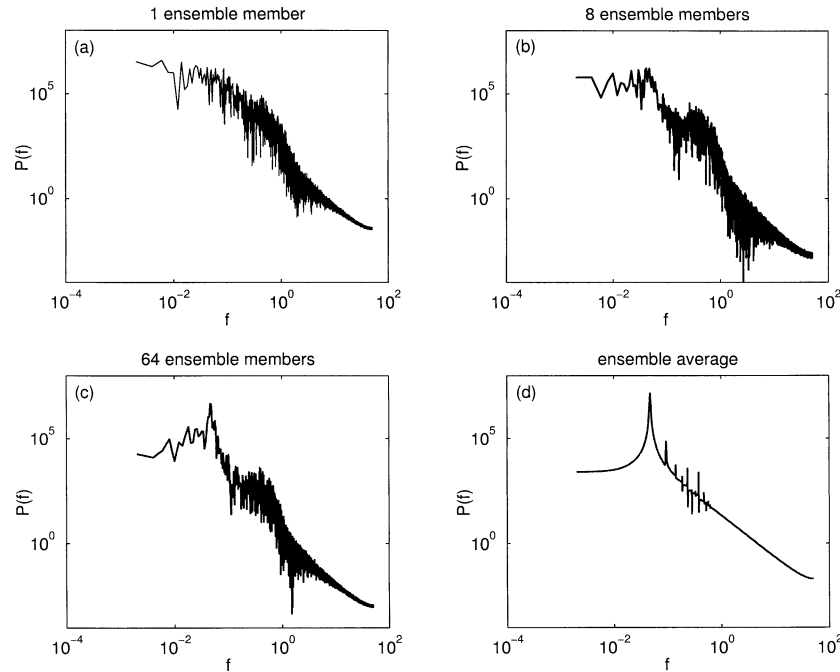
FIG. 16. Power spectrum of the time series of the velocity at the center of the channel $y = 1$ for various numbers of ensemble members as a function of frequency in Hz for the barotropic jet example. Shown are the case of (a) 1 ensemble member, (b) 8 ensemble members (c) 64 ensemble members, and (d) infinite ensemble members. This infinite ensemble case is equivalent to the ensemble mean flow which is in a limit cycle (cf. Fig. 3). Clear indication of the periodic variation of the limit cycle appears with 64 members included in the ensemble.

nonlinear coupled equations with robust and relatively simple behavior. Four fundamental regimes are found: stable symmetric jets, stable asymmetric jets, periodic limit cycles, and chaotic vacillation. These regimes are separated by structural bifurcations; the stable symmetric regime bifurcates with a pitchfork bifurcation to two stable asymmetric states, which bifurcate through a supercritical Hopf bifurcation to a limit cycle.

We further studied the dynamics of these equilibria using examples with finite ensembles, which approached the ensemble mean behavior as the number of ensembles members increases. Earth's midlatitude jet dynamics were found to correspond in structure to the dynamics of a finite ensemble in the stable asymmetric regime with forcing by $O(10)$ ensemble members. In contrast the QBO of the earth's equatorial stratosphere corresponds to ensemble mean dynamics, and the regularity of its period indicates a large ensemble of eddy forcings maintaining it in the stable limit cycle regime. A similar stable limit cycle regime is consistent with the torsional oscillation of the zonal wind observed in the solar convection zone.

Multiple jet equilibria are found in the absence of a strong relaxation back to an imposed equilibrium jet structure in both the stable and vacillating regimes when a sufficient meridional domain is available. This regime is appropriate for the gaseous planets in which turbu-

lence is observed to organize and maintain banded winds.

In addition to structural changes associated with bifurcations in the equations we also find threshold behavior in which a stable jet equilibrium becomes unstable and is no longer supported. The loss of an equilibrium jet as a threshold is passed in the forcing provides an explanation for reorganization of jet structure on timescales short compared with radiative forcing timescales.

An important application of these coupled equations is their interpretation as a theory for equilibration of shear instability. The global stability of the coupled equations is important to this interpretation. Although equilibration is generally found, the equilibrated mean flow may be either steady, periodic, or vacillating irregularly and the instantaneous jet may be episodically unstable.

The coupled equations are stochastic and nonlinear with a wide variety of spatial and temporal scales and yet with remarkable simplicity of behavior in the asymptotic limit of a large number of ensemble members. As the number of ensemble members decreases a descent in idealization occurs with the jet becoming increasingly disrupted while still retaining connection to the underlying asymptotic simplicity.

Some multiple equilibria exist, in particular the jet

example supports multiple equilibria in the asymmetric regime, and examining the first principal component of jet vacillation in the limit cycle regime of the asymptotic system even with as few as five ensemble members retained showed vestiges of this underlying limit cycle. However, in agreement with observations we find no multimodal structure in the pdf with ensemble sizes appropriate for the midlatitude jet. This result shows how multiple equilibria can exist in the underlying asymptotic system and yet not influence the pdf of the complete system or of its individual EOFs. It also demonstrates that careful filtering such as projecting the jet vacillation on its first principal component and then forming the autocorrelation may uncover the underlying order of the asymptotic system.

APPENDIX

Global Stability of the Wave–Mean Flow Equations

We show that the wave–mean flow equations

$$\frac{d\mathbf{C}}{dt} = \mathbf{AC} + \mathbf{CA}^\dagger + \mathbf{Q}, \tag{A1}$$

$$\frac{dU}{dt} = \overline{vq} - r_e(U - U_e), \tag{A2}$$

governing the coupled dynamics in the limit of an infinite ensemble are globally stable.

Without loss of generality transform (A1) to generalized velocity coordinates so that trace $\mathbf{C}$ is the perturbation energy, E_ψ, integrated over the channel:

$$E_\psi = \frac{1}{4} \int_0^L \left(\left| \frac{\partial \hat{\psi}}{\partial y} \right|^2 + k^2 |\hat{\psi}|^2 \right) dy. \tag{A3}$$

The evolution equation for the perturbation energy is

$$\frac{dE_\psi}{dt} = -\int_0^L dy\, U\overline{vq} + F - 2r_1 E_\psi. \tag{A4}$$

The positive term F is the energy injection by the forcing, which for white noise forcing is equal to the trace of the forcing covariance matrix $\mathbf{Q}$.

The mean flow energy equation is obtained by multiplying (A2) by $U(y, t)$ and integrating over the channel:

$$\frac{dE_U}{dt} = \frac{d}{dt} \int_0^L U^2 \, dy$$

$$= \int_0^L U\overline{vq} \, dy - r_e \int_0^L (U^2 - UU_e) \, dy. \tag{A5}$$

Adding the two energy equations we obtain the total energy equation:

$$\frac{d}{dt}(E_U + E_\psi)$$

$$= F - 2r_1 E_\psi - 2r_e E_U + r_e \int_0^L UU_e \, dy. \tag{A6}$$

Noting that

$$\int_0^L UU_e \, dy \le \int_0^L \frac{U^2 + U_e^2}{2} \, dy, \tag{A7}$$

and selecting $r = \min(2r_1, r_e)$ we obtain the inequality for the total energy $E = E_U + E_\psi$:

$$\frac{dE}{dt} \le F + r_e E_e - rE, \tag{A8}$$

where E_e is the kinetic energy of the radiative equilibrium flow U_e. Integrating (A8) we find that the total energy $E = E_U + E_\psi$ at time t is bounded from above:

$$E(t) \le E(0) + \frac{1 - e^{-rt}}{r}(F + r_e E_e). \tag{A9}$$

This expression proves global stability of the coupled dynamical system (A1), (A2). It proves that the total energy is bounded and, hence, separately the energy of the mean flow and of the perturbation field are bounded. Moreover, boundedness of the perturbation energy implies boundedness of all the elements of the covariance matrix, because the sum of the squares of the elements of the positive definite $\mathbf{C}$, that is, the square of the Frobenius norm of $\mathbf{C}$, is smaller[A1] than the square of the trace of $\mathbf{C}$, that is, the perturbation energy E_ψ. Consequently, all the elements of the covariance matrix remain bounded.

Remarks:

1) Global stability is also ensured with very weak relaxation to the radiative equilibrium mean flow U_e, as would be appropriate for the case of the QBO, the solar cycle, or the Jovian winds. With $r_e = 0$ we obtain from (A6)

$$\frac{dE}{dt} = F - 2r_1 E_\psi \le F - 2r_1 E, \tag{A10}$$

from which global stability follows by the previous argument.

2) Global stability is also ensured for time-dependent forcing $F(t)$ with bounded variations, because in that case (A9) is certainly satisfied with the value $F = \max[F(t)]$. In particular this implies that global stability is also ensured for cases in which a finite number of ensemble members are considered as in (8a)–(8c).

[A1] This is because the square of the Frobenius norm is the sum of the squares of the singular values, which for a positive definite matrix are equal to the eigenvalues of the matrix. The trace on the other hand is equal to the sum of the eigenvalues, and the inequality follows.

3) The global stability of the coupled system (A1), (A2) is important because it implies that changes of the mean flow induced by potential vorticity fluxes lead to bounded variations of the mean flow.

4) The coupled system (A1), (A2) may be viewed as a generalization of the Landau equations for the stabilization of unstable equilibria and can be used to investigate stabilization even of initially unstable flow configurations. These equations are generally valid for describing the equilibration of forced dissipative fluid systems.

REFERENCES

Brockett, R. W., 1970: *Finite Dimensional Linear Systems.* Wiley, 244 pp.

Charney, J. G., and J. G. DeVore, 1979: Multiple flow equilibria in the atmosphere and blocking. *J. Atmos. Sci.,* **36,** 1205–1216.

Crawford, J. D., 1991: Introduction to bifurcation theory. *Rev. Mod. Phys.,* **63,** 991–1037.

Dansgaard, W., and Coauthors, 1993: Evidence for general instability of past climate from a 250-Kyr ice-core record. *Nature,* **364,** 218–220.

DelSole, T., 1996: Can quasigeostrophic turbulence be modeled stochastically? *J. Atmos. Sci.,* **53,** 1617–1633.

——, 1999: Stochastic models of shear-flow turbulence with enstrophy transfer to subgrid scales. *J. Atmos. Sci.,* **56,** 3692–3703.

——, 2001a: A simple model for transient eddy momentum fluxes in the upper troposphere. *J. Atmos. Sci.,* **58,** 3019–3035.

——, 2001b: A theory for the forcing and dissipation in stochastic turbulence models. *J. Atmos. Sci.,* **58,** 3762–3775.

——, and B. F. Farrell, 1995: A stochastically excited linear system as a model for quasigeostrophic turbulence: Analytic results for one- and two-layer fluids. *J. Atmos. Sci.,* **52,** 2531–2547.

——, and ——, 1996: The quasi-linear equilibration of a thermally maintained, stochastically excited jet in a quasigeostrophic model. *J. Atmos. Sci.,* **53,** 1781–1797.

Dunkerton, T. J., 1997: The role of gravity waves in the quasi-biennial oscillation. *J. Geophys. Res.,* **102,** 26 053–26 076.

Farrell, B. F., and P. J. Ioannou, 1993a: Stochastic dynamics of baroclinic waves. *J. Atmos. Sci.,* **50,** 4044–4057.

——, and ——, 1993b: Stochastic forcing of the linearized Navier–Stokes equations. *Phys. Fluids A,* **5,** 2600–2609.

——, and ——, 1994: A theory for the statistical equilibrium energy and heat flux produced by transient baroclinic waves. *J. Atmos. Sci.,* **51,** 2685–2698.

——, and ——, 1995: Stochastic dynamics of the mid–latitude atmospheric jet. *J. Atmos. Sci.,* **52,** 1642–1656.

——, and ——, 1996: Generalized Stability. Part I: Autonomous Operators. *J. Atmos. Sci.,* **53,** 2025–2041.

——, and ——, 1998: Perturbation structure and spectra in turbulent channel flow. *Theor. Comput. Fluid Dyn.,* **11,** 215–227.

——, and ——, 2002: Perturbation growth and structure in uncertain flows: Part II. *J. Atmos. Sci.,* **59,** 2647–2664.

Feldstein, S. B., 2000: Is interannual zonal mean flow variability simply climate noise? *J. Atmos. Sci.,* **57,** 2356–2362.

——, and S. Lee, 1998: Is the atmospheric zonal index driven by an eddy feedback? *J. Atmos. Sci.,* **55,** 3077–3086.

Guckenheimer, J., and P. Holmes, 1983: *Nonlinear Oscillations, Dynamical Systems, and Bifurcations of Vector Fields.* Springer-Verlag, 453 pp.

Gutowski, W. J., 1985: Baroclinic adjustment and midlatitude temperature profiles. *J. Atmos. Sci.,* **42,** 1733–1745.

Hartmann, D. L., 1995: A PV view of zonal flow vacillation. *J. Atmos. Sci.,* **52,** 2561–2576.

——, and F. Lo, 1998: Wave-driven zonal flow vacillation in the Southern Hemisphere. *J. Atmos. Sci.,* **55,** 1303–1315.

Holton, J. R., and C. Mass, 1976: Stratospheric vacillation cycles. *J. Atmos. Sci.,* **33,** 2218–2225.

Hou, A. Y., and B. F. Farrell, 1987: Superrotation induced by critical-level absorption of gravity waves on Venus: An assessment. *J. Atmos. Sci.,* **44,** 1049–1061.

Ingersol, A. P., 1990: Atmospheric dynamics of the outer planets. *Science,* **248,** 308–315.

Ioannou, P. J., and R. S. Lindzen, 1994: Gravitational tides in the outer planets. Part III: Atmospheric response and mean flow acceleration. *Astrophys. J.,* **424,** 1005–1013.

Karoly, D. J., 1990: The role of transient eddies in the low frequency zonal variations in the Southern Hemisphere. *Tellus,* **42A,** 41–50.

Kidson, J. W., and M. R. Sinclair, 1995: The influence of persistent anomalies on Southern Hemisphere storm tracks. *J. Climate,* **8,** 1938–1950.

Koo, S., A. W. Robertson, and M. Ghil, 2002: Multiple regimes and low frequency oscillations in the Southern Hemisphere's zonal-mean flow. *J. Geophys. Res.,* **107,** 4596–4609.

Lee, S., and S. B. Feldstein, 1996: Mechanisms of zonal index evolution in a two layer model. *J. Atmos. Sci.,* **53,** 2232–2246.

Lindzen, R. S., and J. R. Holton, 1968: A theory of the quasi-biennial oscillation. *J. Atmos. Sci.,* **25,** 1095–1107.

——, and B. Farrell, 1977: Some realistic modifications of simple climate models. *J. Atmos. Sci.,* **34,** 1487–1501.

——, ——, and D. Jacqmin, 1982: Vacillations due to wave interference: Applications to the atmosphere and to annulus experiments. *J. Atmos. Sci.,* **39,** 14–23.

Lorenz, D. J., and D. L. Hartmann, 2001: Eddy–zonal flow feedback in the southern hemisphere. *J. Atmos. Sci.,* **58,** 3312–3327.

Panetta, R. L., 1993: Zonal jets in wide baroclinically unstable regions: Persistence and scale selection. *J. Atmos. Sci.,* **50,** 2073–2106.

Pedlosky, J., 1972: Limit cycles and unstable baroclinic waves. *J. Atmos. Sci.,* **29,** 53–63.

——, 1977: A model of wave amplitude vacillation. *J. Atmos. Sci.,* **34,** 1898–1912.

——, and C. Frenzen, 1980: Chaotic and periodic behavior of finite amplitude baroclinic waves. *J. Atmos. Sci.,* **37,** 1176–1196.

Plumb, R. A., and A. D. McEwan, 1978: The instability of a forced standing wave in a viscous stratified fluid. *J. Atmos. Sci.,* **35,** 1827–1839.

Reed, R. J., and D. G. Rogers, 1962: The circulation of the lower stratosphere in the years 1954–1960. *J. Atmos. Sci.,* **19,** 127–135.

Robinson, W. A., 1991: The dynamics of the zonal index in a simple model of the atmosphere. *Tellus,* **43A,** 295–305.

——, 1996: Does eddy feedback sustain variability in the zonal index? *J. Atmos. Sci.,* **53,** 3556–3569.

——, 2000: A baroclinic mechanism for the eddy feedback on the zonal index. *J. Atmos. Sci.,* **57,** 415–422.

Schoeberl, M. R., and R. S. Lindzen, 1984: A numerical simulation of barotropic instability. Part I: Wave–mean flow interaction. *J. Atmos. Sci.,* **41,** 1368–1379.

Scott, R. K., and P. H. Haynes, 2000: Internal vacillations in stratosphere-only models. *J. Atmos. Sci.,* **57,** 3233–3250.

Stone, P. H., 1978: Baroclinic adjustment. *J. Atmos. Sci.,* **35,** 561–571.

Vorontsov, S. V., J. Christensen-Dalsgaard, J. Schou, V. N. Strakhov, and M. J. Thompson, 2002: Helioseismic measurement of solar torsional oscillations. *Science,* **296,** 101–103.

Watterson, I. G., 2002: Wave–mean flow feedback and the persistence of simulated zonal flow vacillation. *J. Atmos. Sci.,* **59,** 1274–1288.

Williams, G. P., 1979a: Planetary circulations: 2. The Jovian quasi-geostrophic regime. *J. Atmos. Sci.,* **36,** 932–968.

——, 1979b: Planetary circulations: 3. The terrestrial quasi-geostrophic regime. *J. Atmos. Sci.,* **36,** 1409–1435.

Whitaker, J. S., and P. D. Sardeshmukh, 1998: A linear theory of

extratropical synoptic eddy statistics. *J. Atmos. Sci.,* **55,** 237–258.

Yoden, S., 1987a: Bifurcation properties of a stratospheric vacillation model. *J. Atmos. Sci.,* **44,** 1723–1733.

——, 1987b: Dynamical aspects of stratospheric vacillations in a highly truncated model. *J. Atmos. Sci.,* **44,** 3683–3695.

Zhang, Y., and I. Held, 1999: A linear stochastic model of a GCM's midlatitude storm tracks. *J. Atmos. Sci.,* **56,** 3416–3435.